Critical-current anisotropy due to inclined and crossed linear defects

Thomas Schuster and Holger Kuhn
Max-Planck-Institut für Metallforschung, Institut für Physik, Postfach 800665, D-70506 Stuttgart, Germany

Mikhail Indenbom*
Institut de Génie Atomique, Ecole Polytechnique Fédérale de Lausanne, CH-1015 Lausanne, Switzerland

Martino Leghissa and Michael Kraus
III. Physikalisches Institut, Universität Erlangen-Nürnberg, Erwin-Rommel-Straße 1, D-91058 Erlangen, Germany

Marcin Konczykowski
Laboratoire des Solides Irradiés, Ecole Polytechnique, 91128 Palaiseau, France
(Received 10 January 1995)

Parallel linear defects which are inclined to the sample surface normal and crossed linear defects are introduced into $DyBa_2Cu_3O_{7-\delta}$ and $Bi_2Sr_2CaCu_2O_{8+\delta}$ single crystals by high-energy heavy-ion irradiation. The dependence of flux penetration on temperature, fluence, and applied external magnetic field is investigated before and after irradiation. For crossed linear defects much higher pinning than for parallel defects with the same density is observed for both materials. This finding is attributed to the intersections of linear defects which allow the flux lines to be more effectively pinned than by parallel defects. In this case flux-line depinning occurs by kink-pair nucleation in the sample volume as in the Bose-glass model. From parallel linear defects the flux lines may be more easily depinned by nucleation of surface kinks. The observed low anisotropy $j_\parallel/j_\perp \approx 2$ of the critical current flowing parallel or perpendicular, respectively, to the inclination plane of the defects in parallel-irradiated $DyBa_2Cu_3O_{7-\delta}$ is explained by different geometrical arrangement of defects and flux lines in the directions of flux-line motion. During field decrease the anisotropy is found to disappear in samples with parallel linear defects. For crossed defects the anisotropy $j_\parallel/j_\perp \approx 2$ reverses in decreasing field since the flux lines are effectively pinned only in the inclination plane of the linear defects. In $Bi_2Sr_2CaCu_2O_{8+\delta}$ single crystals the flux penetration is isotropic; this is understood from the pancake-vortex model. The different observations in $DyBa_2Cu_3O_{7-\delta}$ and $Bi_2Sr_2CaCu_2O_{8+\delta}$ single crystals are in good agreement with a recently given scaling approach.

I. INTRODUCTION

One of the most interesting features of high-T_c superconductors (HTSC's) for both applications and theoretical understanding is the pinning of flux lines (FL's) at sample inhomogeneities. Pinning causes a strongly nonlinear current-voltage characteristic of the superconductor which is described by essentially two parameters, the critical-current density j_c at which the Abrikosov FL's depin at $T = 0$ and start to move under the influence of the Lorentz force and the activation energy U. The resulting flux penetration is well described by model calculations using a current-voltage law, e.g., of the form $E \sim (j/j_c)^n$, in all regimes from thermally activated flux flow ($n = 1$) to the classical Bean model ($n \gg 1$) (see Ref. 1), where E is the electric field and the exponent n is determined by U.[1]

Very effective pinning centers are linear defects (LD's) with a radius of the nonsuperconducting core[2] $R \approx \sqrt{2}\xi$ where ξ is the coherence length. In HTSC's such defects can be introduced by high-energy heavy-ion irradiation.[3] Various groups[4–11] report an irradiation-induced shift of the irreversibility line (IL) to higher temperatures T and higher magnetic flux densities B and an enhancement of j_c. The existence of LD's in superconductors in which the density, extension, and direction of linear defects are known allows one to identify specific depinning mechanisms of the flux-line lattice (FLL) to be investigated. At low temperatures the small enhancement of U by the introduction of LD's into $Bi_2Sr_2CaCu_2O_{8+\delta}$ (Bi2212) single crystals[8,9] and $(Bi,Pb)_2Sr_2Ca_2Cu_3O_{10+\delta}$-Ag (Bi2223) tapes[12] was attributed to Clem's pancake vortex model.[13] However, in the three-dimensional (3D) HTSC's $DyBa_2Cu_3O_{7-\delta}$ (DBCO) (Ref. 10) and $YBa_2Cu_3O_{7-\delta}$ (YBCO) (Refs. 14, 15) it was suggested that this behavior may be explained by the low energy of vortex-kink formation between LD's.[16] Using the Träuble-Essmann decoration technique[17] to visualize the FLL Leghissa *et al.*[18] and Dai *et al.*[19] found a highly disordered vortex state due to randomly distributed, very effective linear pins in Bi2212 single crystals. Theoretical treatments of FL pinning in samples with LD's using a Bose-glass model and their application to experimental findings are given in Refs. 16 and 20–23.

To get a deeper insight into FL pinning and depinning, in particular when the FL's are aligned parallel or inclined to the LD's, magnetization measurements were performed using superconducting quantum interference

devices (SQUID's) or vibrating sample magnetometers (VSM's). These investigations were carried out on samples with LD's generated by oblique irradiation with respect to the c axis, which is oriented perpendicular to the sample surface. In YBCO Civale *et al.*[5] observed that the j_c enhancement is large when the applied magnetic field H_a is aligned with the LD's, whereas only a small enhancement is observed when the LD's deviate from the magnetic field direction. The same result was found by Kraus *et al.*[24] for DBCO single crystals which were prepared by the same procedure as the crystals investigated in this paper. However, Thompson *et al.*[25] did not find such an effect in Bi2212 single crystals at low temperatures. Similar experiments were performed by Klein *et al.*[26] who observed a difference in the j_c enhancement in Bi2212 single crystals for the different directions of H_a parallel and inclined to the LD's at $T > 50$ K, whereas the same behavior as reported in Ref. 25 was found for $T < 50$ K. This was attributed to a crossover from two-dimensional (2D) to 3D vortices in such samples near $T = 50$ K. Such a 2D-3D crossover was also observed in Bi2223 tapes by Kummeth *et al.*[12]

Similar experiments to the ones reported in Ref. 5 were done by Prozorov *et al.*[28] on obliquely irradiated YBCO thin films. Angular-dependent four-terminal measurements on YBCO thin films and YBCO/$PrBa_2Cu_3O_{7-\delta}$ (PBCO) superlattices after oblique irradiation were performed by Holzapfel *et al.*[29] who found a larger increase of j_c for H_a aligned parallel to the LD's than for H_a aligned parallel to the Cu-O layers in YBCO. In YBCO/PBCO superlattices the absence of this behavior was explained by the decoupling of FL's into pancake vortices in the superlattices. Investigations of vortices inclined to the LD's by a large angle are of particular interest if one wants to produce nonparallel LD's in order to increase j_c and the irreversibility temperature T_{irr} above that of parallel LD's.[22,27] FL's inclined to LD's by large angles cannot be described in the framework of the Bose-glass model and an extended theory is required.[30]

Since the magnetization measurements yield only an integral signal of currents flowing in all directions in the sample, a correct interpretation of the data is not easy, especially if one has to account for large demagnetization effects or (when the sample is rotated) for a misalignment of the total magnetic moment and the apparatus axis. A powerful tool to avoid these difficulties is provided by local investigations of flux distributions using the magneto-optical Faraday effect. In such experiments different modes of FL motion parallel and perpendicular to the LD's and two different critical currents densities $j_\perp$ and $j_\parallel$ flowing perpendicular and parallel to the projection of the LD's on the sample surface are directly visualized and can be measured simultaneously.[31] In this way we are able to investigate properties of the FLL and to obtain a better understanding of the behavior of FL motion through a forest of LD's.

In this paper we present magneto-optical observations of flux distributions in DBCO and Bi2212 single crystals after oblique irradiation with high-energy heavy ions. We performed detailed investigations of the T, B, fluence, and angular dependence of the irradiation-induced critical-current anisotropy. The obtained results are compared with integral magnetization measurements and new mechanisms for FL depinning from LD's are presented.

II. EXPERIMENTS

A. Faraday effect

We visualize the magnetic field distribution of a superconductor by magneto-optics. Since the HTSC's themselves have no significant magneto-optical effect, the sample surfaces have to be covered by a magneto-optically active material. For our investigations we use the magneto-optical Faraday effect. The flux penetration is imaged by detecting the rotation of the polarization plane when linearly polarized light passes a magneto-optically active layer exposed to the magnetic field of the underlying superconductor. From flux-free regions the light is reflected without rotation of the polarization plane; this light thus cannot pass an analyzer which is set in a crossed position with respect to the polarizer. In this way the Shubnikov phase (with a flux-line lattice) will be imaged as bright areas, whereas the flux-free Meissner phase remains dark.

For the experiments presented in this paper our indicators were EuSe thin films and ferrimagnetic iron-garnet films with an in-plane anisotropy. The EuSe thin films were deposited by electron-beam evaporation directly onto the sample surface, which was coated before with an aluminum layer (thickness about 200 nm), in order to enhance its reflectivity.[32] This technique allows flux distributions to be observed directly with a spatial resolution of about 1 μm in a temperature range of 5 K $\leq T \leq$ 20 K. The lower-temperature boundary is given by the cryostat, while the upper limit is imposed by the temperature dependence of the Verdet constant of the europium chalcogenides, which means very low rotation angles at higher temperatures.[33] Anyway, flux distributions at temperatures above 20 K can be visualized indirectly by a special procedure during which the flux distribution existing at a given temperature is observed after cooling the sample down to 5 K. This technique gives the correct flux patterns because j_c becomes larger when the temperature is decreased; therefore, the sample at lower temperatures enters an undercritical state; i.e., the flux distribution is not changed.[34]

The iron-garnet film was grown by liquid phase epitaxy onto a gallium-gadolinium substrate with a thickness of about 3.5 μm (commercial firm Gamma Scientific Production, Russia).[35] This kind of indicator allows the flux penetration into HTSC samples to be observed directly in the whole temperature regime of superconductivity with a higher magnetic sensitivity than with the EuSe thin films. However, its spatial resolution is limited by the thickness of the indicator to about 4 μm. The superconductor was glued onto this substrate by the carbon cement "Leit-C."

The external magnetic field is generated by a copper solenoid coil, which is cooled with liquid nitrogen and produces a maximum field of 0.55 T. The observations

were performed in the optical cryostat described in Refs. 32 and 36. All images can be observed directly via the microscope or be transferred to an image processing system for analyzing.[37] The image processing system allows one to determine the grey level pixel by pixel along a user-defined line.

B. Sample preparation and irradiation

The Bi2212 single crystals investigated here were prepared by the traveling-solvent floating-zone method as described in Ref. 38 with dimensions of about 2 × 2 mm^2 and about 20 μm thickness. The composition of the crystals was determined by electron probe microanalysis to $Bi_{2.16}Sr_{1.91}Ca_{1.03}Cu_2O_{8+x}$ and from ac susceptibility measurements the superconducting critical temperature was determined to $T_c = 88$ K with a transition width of $\Delta T_c = 2.2$ K.

The DBCO single crystals were grown as described in Ref. 39. The crystal dimensions are about 500 × 500 × 15 μm^3 and $T_c = 91$ K as measured by the Meissner effect using SQUID magnetometry. All crystals have a distinct twin structure which was revealed by polarized light microscopy.

Inclined LD's were introduced by irradiation with 0.9-GeV Pb ions at GANIL (Caen, France) or, respectively, with 500-MeV Xe ions at the ISL accelerator (Hahn-Meitner-Institut, Berlin, Germany). The samples were glued on copper sample holders and mounted at various angles φ between the ion beam and the surface normal, i.e., the c axis of the sample. For all kinds of irradiation experiments the fluences were in the range $\phi t = 0.1$–3.8×10^{11} ions/cm^2 and the inclination direction was set parallel to the longer crystal edges. Parallel LD's were introduced at $\varphi = 0°$, 30°, and 45°, whereas crossed LD's were produced by directing the ion beam first at $\varphi = 45°$ and subsequently at $-45°$, i.e., from the opposite side to the sample surface; see Fig. 1. The range of both projectiles in the target material is larger than the sample thickness. The heavy-ion irradiation lowers the critical temperature T_c by about 2 K at the fluences used.

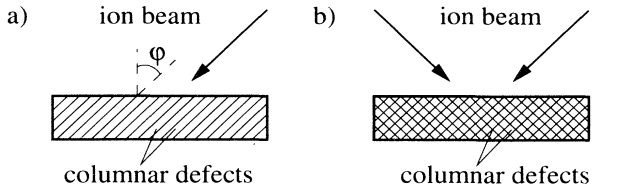

FIG. 1. Sketch of the angular irradiation. (a) Irradiation introducing parallel LD's which are inclined to the sample surface. (b) Production of crossed LD's by directing the ion beam at $\varphi = +45°$ and $\varphi = -45°$ to the sample-surface normal.

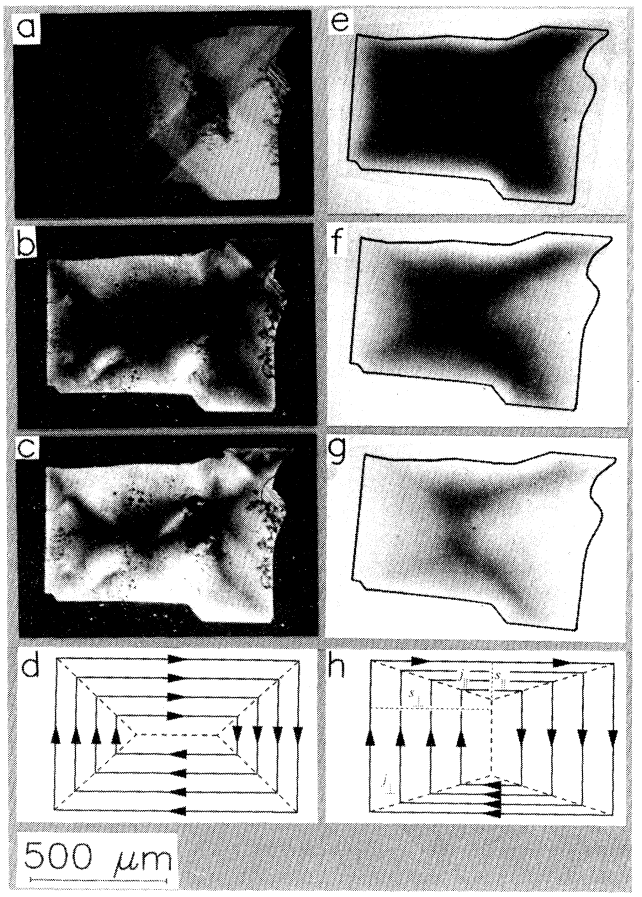

FIG. 2. Flux distributions in a DBCO single crystal before and after irradiation with 500-MeV Xe ions at $\varphi = 45°$ and $\phi t = 1.29 \times 10^{11}$ ions/cm^2. The observation temperature is $T = 30$ K before (b), (c) and $T = 60$ K after irradiation (e)–(g). (a) Polarization micrograph of the crystal surface before coating with the Al and EuSe layers. The twin structure is visible as straight lines running at 45° to the sample edges. (b) $\mu_0 H_a = 171$ mT, (c) 256 mT. The flux distributions before irradiation were visualized using a EuSe thin film. (d) Isotropic current distribution in a rectangular sample in the critical state. (e) $\mu_0 H_a = 85$ mT. The flux distributions after irradiation were revealed using a ferrimagnetic iron-garnet indicator. (f) 171 mT, (g) 256 mT, (h) anisotropic current distribution in a rectangular sample. The ratio $j_\parallel / j_\perp$ of the critical currents flowing parallel or perpendicular to the LD's can be determined by measuring the distances $s_\parallel$ and $s_\perp$.

III. RESULTS AND DISCUSSION

A. Irradiation-induced critical-current anisotropy in DBCO

Figure 2(a) shows a polarization micrograph of the surface of a DBCO single crystal before coating it with the magneto-optical indicator layer. All DBCO single crystals under study here have a distinct twin structure which is visible as straight lines running under an angle of 45° to the sample edges. The visualization of the twin structure is due to the quasi-one-dimensional optical conductivity of DBCO.[40] In a polarization microscope the corresponding phase shift of light with its polarization plane parallel to the crystallographical b axis results in different intensities of regions with different twin orientations. The c axis of the sample is perpendicular to the sur-

face and hence parallel to the external magnetic field. The flux distributions before irradiation obtained at $T = 30$ K in applied perpendicular fields of $\mu_0 H_a = 171$ mT and 256 mT are depicted in Figs. 2(b) and 2(c), respectively. The white areas are the Shubnikov phase whereas the flux-free Meissner phase remains dark. We observe a cushionlike[41,10] flux penetration slightly disturbed by the influence of the twin structure, which is visible as bright lines of enhanced flux density. In the critical state [Fig. 2(c)] the flux pattern exhibits the typical double-Y structure aligned parallel to the longer sample edge as expected from an isotropic critical-current distribution. For a rectangular sample in the critical state the isotropic current distribution is drawn in Fig. 2(d). Here, a critical current of constant density j_c flows in the whole superconductor. A characteristic feature of such a vector field with a constant absolute value of the vector is the formation of sharp bends in the streamlines;[42] this was discussed for type-II superconductors in the review by Campbell and Evetts.[43] The bends occur at discontinuity lines (d lines) of the current and divide the superconductor into domains with uniform parallel current flow. The characteristics of the d lines under various geometric conditions and their experimental observation were described recently in Ref. 44. To fulfill the continuity condition for the critical current, the d lines form an angle of 45° with the edges of the rectangular sample in the isotropic case. This indeed is approximately the situation presented in Fig. 2(c) showing that the pinning force density was isotropic before irradiation.

The flux distributions after irradiation with 500-MeV Xe ions at $\phi t = 1.29 \times 10^{11}$ ions/cm^2 are visualized using a ferrimagnetic iron-garnet indicator because the EuSe layer was soiled during preparation for the irradiation. The ion beam was directed parallel to the longer crystal edge and inclined to its surface by $\varphi = 45°$. The flux patterns obtained at $T = 60$ K are shown in Figs. 2(e)–2(g) for $\mu_0 H_a = 85$ mT, 171 mT, and 256 mT, respectively. The black frames mark the crystal edges. The flux penetration differs considerably from the one observed in the unirradiated crystal: Along the introduced LD's, i.e., from the left and right sample edges, we find a deeper flux penetration than perpendicular to the defect orientation. Therefore, the double-Y structure of the d lines in the critical state [Fig. 2(g)] is now oriented perpendicular to the longer sample side, in contrast to the unirradiated crystal as already reported in our recent paper.[31] This behavior was found to be a characteristic feature for an anisotropic distribution of j_c (Ref. 45) as depicted in Fig. 2(h). Here, the different current densities $j_\parallel$ and $j_\perp$ flowing parallel or perpendicular, respectively, to the LD's are symbolized by different densities of parallel, equidistant streamlines. The ratio $j_\parallel/j_\perp$ can be determined by measuring $s_\parallel$ and $s_\perp$, which are the distances of flux penetration depth from the sample edge to the central d line in the two directions in the critical state. From the current continuity equation follows $j_\parallel/j_\perp = s_\perp/s_\parallel$. From Fig. 2(g) we obtain $j_\parallel/j_\perp \approx 2$, which is approximately the same as for the crystal investigated in Ref. 31 (0.9-GeV Pb ions, $\varphi = 45°$, $\phi t = 1.41 \times 10^{11}$ ions/cm^2). Due to the spatial resolution of the ferrimagnetic iron-garnet indicator, the absolute error of the distances $s_\parallel$ and $s_\perp$ is 4 μm, and thus the relative error of the anisotropy ratio is about 1%. In this way we are able to determine ratios of current densities with high accuracy although the absolute values of the current densities can be determined only inaccurately by magneto-optics.[44] For the anisotropy ratio we measured $s_\perp$ in the left domain as indicated in Fig. 2(h); the difference of the flux-penetration depths from the left and right sample edges will be discussed later. An anisotropic flux penetration was also observed for the crystals irradiated at $\varphi = 30°$.

In Fig. 3(a) depinning processes of FL's from LD's are shown. The LD's are drawn as cylinders; the FL's are

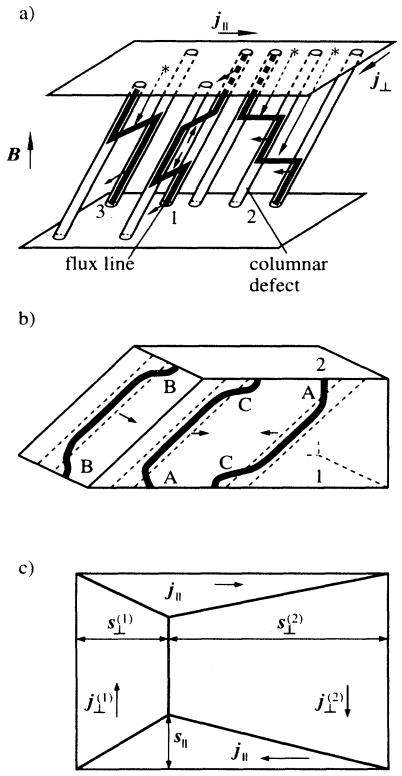

FIG. 3. (a) Sketch of three different modes of vortex motion parallel and perpendicular to the inclination direction of the LD's. Process 1: vortex motion perpendicular to the LD's forced by $j_\parallel$. It is possible only after thermal activation and spread of kink pairs in the sample volume. Process 2: vortex motion in the inclination direction of the LD's by kink sliding forced by $j_\perp$. For a continuous motion kink nucleation at the surface is needed. Process 3: perpendicular motion as for process 1 but due to kink nucleation at the surface which is easier than kink-pair nucleation. The direction of vortex and kink motion are indicated by arrows. (b) Kink nucleation at the surface for vortex motion parallel (process 2) and perpendicular (process 3) to the LD's. The nucleation energy is largest for nucleation mode C and smallest for nucleation mode A. (c) Current distribution and topology of d lines for a sample with an anisotropy $j_\parallel/j_\perp$ due to inclined LD's and a difference in $j_\perp$ which is additionally to the case shown in Fig. 2(h) due to different surface qualities.

bold lines. Most of each FL is pinned by the LD's and only the FL kinks which connect FL segments pinned in adjacent LD's can move easily along the LD's. In infinitely extended samples depinning can occur only by kink pair nucleation in the volume (process 1), as considered by Brandt[46] and in the statistical theory of thermal depinning from randomly distributed LD's (Refs. 16, 21) (Bose-glass model). These theories were developed for parallel FL's and LD's where the motions in all directions are equivalent. However, in real experimental situations the FL's, which are usually curved due to demagnetization field, are inclined to the LD's and one of the basic assumptions, that a FL is pinned by *one* LD, is violated. In this case, the FL's have to form kinks from one LD to another which can slide easily along the LD's as depicted in Fig. 3(a) for process 2. The sliding of kinks along the LD's is impeded only by the background pinning which is present already before irradiation and $j_\perp$ should not be affected by introduction of LD's. Thus, for oblique irradiation, we can conclude that the observed anisotropy $j_\parallel/j_\perp$ is due to the different depinning processes 1 and 2 sketched in Fig. 3(a). From the above considerations we expect a huge anisotropy ratio $j_\parallel/j_\perp \approx 30$ at $T = 60$ K (this is the ratio between the critical-current densities in irradiated and unirradiated crystals), whereas the experiment yields only a ratio $j_\parallel/j_\perp \approx 2$; this tells us that this explanation is oversimplified.

The finding that even $j_\perp$ is considerably enhanced by the LD's and becomes comparable to $j_\parallel$ may be due to the following two reasons:

(1) The radius of the LD's may vary along the defect; this "sausaging" impedes the free sliding of kinks.

(2) The continuous kink sliding and the maintainance of the magnetic field direction need kink nucleation at the sample surface. Simple kinks cannot nucleate by fluctuations in the volume but may be produced at the sample surface; only kink pairs can nucleate in the volume. When the FL's are strongly curved, e.g., in decreasing H_a, then other features of FL motion come into play. This is discussed in Sec. III D.

The first reason is rather unlikely because the fluctuations of the diameter of the LD's are too small compared with the coherence length ξ and cannot cause the measured ratio $j_\parallel/j_\perp = 2$. Furthermore, the shape of the LD's produced by 0.9-GeV Pb and 500-MeV Xe is quite different. For a continuous projectile track in DBCO an electronic energy loss S_e of at least 2500 eV/Å is required.[3] Since $S_e = 4500$ eV/Å for 0.9-GeV Pb but only 2840 eV/Å for 500-MeV Xe, the surface of the LD's produced by the latter projectile is much rougher than for Pb irradiation. However, we observe the same anisotropy ratio $j_\parallel/j_\perp \approx 2$ for both projectiles and may thus exclude reason (1) given above. Instead we suggest that the impeding force for kink sliding is due to an energy barrier for kink nucleation at the surface. If we assume that the energy for nucleation of a kink at the surface is only half of that for a kink pair, we conclude that the surface kink nucleation plays the main role also for flux motion perpendicular to the LD's, which is induced by $j_\parallel$. As depicted in Fig. 3(b) we consider three different modes of kink nucleation at the sample surface:

(A) Kink nucleation across the acute angle between the surface and LD. This nucleation energy is lowest because the FL can be shortened by forming a kink.

(B) Kink nucleation perpendicular to the inclination direction. The FL now has to be elongated to reach the neighbored defect and thus the nucleation energy is larger than for mode A.

(C) Kink nucleation at the obtuse angle between surface and LD in the sliding direction. In this case the nucleation energy is largest and therefore mode C does not play a role for FL motion.

The anisotropy $j_\parallel/j_\perp$ is thus expected to be due to the different nucleation energies for kink-production modes A and B which are responsible for the two FL motions parallel and perpendicular, respectively, to the inclination direction of the LD's. For FL motion from left to right the kinks will nucleate at the lower surface 1, whereas for FL motion from right to left the kinks nucleate at the upper surface 2. Thus, different surface qualities, e.g., due to the carbon cement at the lower, the evaporated aluminum layer on the upper surface, or different diameters of the LD's at the two surfaces, should cause different potentials for kink nucleation and induce an additional anisotropy in $j_\perp$ for flux penetration from opposite sides. Such an anisotropy is indeed seen in Fig. 2(g) where the double-Y structure is not exactly centered but shifted towards the side where $j_\perp$ is larger. From Fig. 2(g) we obtain $j_\parallel/j_\perp^{(1)} = 2.0$ for kink nucleation at surface 1 and $j_\parallel/j_\perp^{(2)} = 2.8$ for kink nucleation at surface 2. For this case the current distribution is sketched in Fig. 3(c). An anisotropy ratio $j_\perp^{(1)}/j_\perp^{(2)} \neq 1$ was observed for all our 20 DBCO single crystals after oblique irradiation.

In a brief summary, the above magneto-optical observations of an oblique-irradiation-induced anisotropy of the critical current for vortices moving parallel and perpendicular to the LD's, and also of vortices moving parallel to the LD's when they penetrate from opposite sample edges, indicate that kink nucleation at the sample surface may be the dominant process for FL depinning from LD's. The experiments presented in the following section support these considerations.

The magneto-optically observed anisotropy is in fact different as a matter of principle from the anisotropy observed by magnetization measurements reported in Refs. 5, 15, and 24. Whereas our magneto-optic distinguishes different modes of vortex motion, measurements of magnetic moments $M(\theta)$ at different angles θ between the LD's and the externally applied magnetic field H_a mix the angular dependences of $j_\parallel$ and $j_\perp$. $M(\theta)$ is a superposition of the magnetic moments caused by $j_\parallel$ and $j_\perp$ (or even $j_\parallel$, $j_\perp^{(1)}$, and $j_\perp^{(2)}$), $M(\theta) = \alpha(\theta) j_\parallel(\theta) + \beta(\theta) j_\perp(\theta)$, where the geometrical coefficients α and β in general depend also on the ratio $j_\parallel/j_\perp$. Furthermore, when H_a is inclined to the surface normal of the sample one has to bear in mind that the parallel component of H_a induces a barrier for the crossflow of vortices with different orientations.[47,48] This causes an additional anisotropy[49] which superimposes the effects described above. Therefore, we performed our magneto-optical experiments with H_a aligned perpendicular to the sample surface in order

to ensure a well-defined experimental environment.

A further interesting result of our investigations is that the influence of twin boundaries as channels of preferred flux penetration completely disappears after heavy-ion irradiation. This means that twin boundaries do not reduce the superconductivity but only modify the pinning behavior; namely, pinning is weak for flux penetration along the twin boundaries and strong for perpendicular penetration. Boundaries between regions of different twin orientations produce high internal stresses in the superconductor, which reduce the number of oxygen vacancies and other point defects considerably. Such boundaries are thus the most preferred channels for flux penetration in as-grown DBCO (and YBCO) single crystals. Typically this easy channeling is most effective at intermediate temperatures.[50] By introducing LD's this pinning modulation is completely masked. This would be impossible in the case of real weak links due to suppressed superconductivity. The disappearance of the influence of twin boundaries on flux distributions after heavy-ion irradiation was also observed in single crystals containing LD's perpendicular to their surfaces.

In order to enhance the critical-current density further we performed irradiation experiments which produce crossed LD's as sketched in Fig. 1(b). The kink sliding is now stopped at all intersections of the LD's; see Fig. 4. If the oversimplified explanation (kink sliding–kink pair) of the $j_\parallel/j_\perp$ anisotropy for inclined LD's presented in Fig. 3(a) works, the current anisotropy should disappear in the presence of crossed LD's.

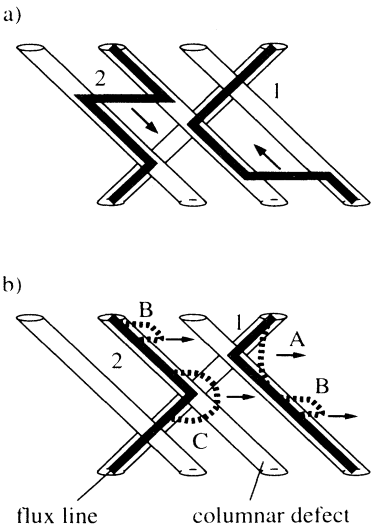

FIG. 4. Sketch of vortex motion in presence of crossed LD's. (a) Kinks of vortices 1 and 2 which are pinned by crossed LD's slide along the LD's. (b) The kinks of vortices 1 and 2 are pinned by the next intersection of the LD's. The vortex bend of FL 2 at the LD intersection is more strongly pinned than the one of FL 1 which can be depinned in its sliding direction. The difference between the two depinning modes A and C here is due to geometry which is somewhat similar to the difference of modes A and C in Fig. 3(b). The depinning mode B by usual kink-pair nucleation is equal along the inclination direction of the LD's and perpendicular to them and requires an intermediate energy. The possible modes of depinning are indicated by dashed vortex lines.

B. Crossed linear defects in DBCO

To observe the flux distribution in the critical state in a wider temperature range we irradiated DBCO crystals with 0.9-GeV Pb ions at a low fluence $\phi t = 1.0\times10^{10}$ ions/cm^2. The irradiation angle was $\varphi = \pm45°$ to produce crossed linear defects; see Fig. 1(b). From such a low fluence we expect a lower j_c enhancement than in the previous section, because the j_c enhancement is strongly dependent on the irradiation fluence. For example, Gerhäuser *et al.*[8] found a j_c which is 5 times higher for $\phi t = 1.5 \times 10^{11}$ ions/cm^2 than for 2×10^{10} ions/cm^2 in Bi2212 single crystals at $T = 10$ K and $\mu_0 H_a = 0.5$ T. However, as will be shown below, the decrease of j_c with increasing temperature is considerably lower for cross-irradiated samples than for parallel-irradiated ones; with equal fluences it would thus be impossible with our experimental setup to compare j_c of both kinds of irradiation in the same temperature range.

Figure 5 shows the flux penetration into a cross-irradiated DBCO single crystal for (a) $\mu_0 H_a = 43$ mT, (b) 85 mT, (c) 128 mT, and (d) 213 mT. The flux distributions were visualized using a ferrimagnetic iron-garnet indicator at $T = 60$ K and H_a is aligned parallel to the surface normal, i.e., the c axis of the crystal. The black frame marks the sample edges. We observe an anisotropic current distribution; namely, the flux pen-

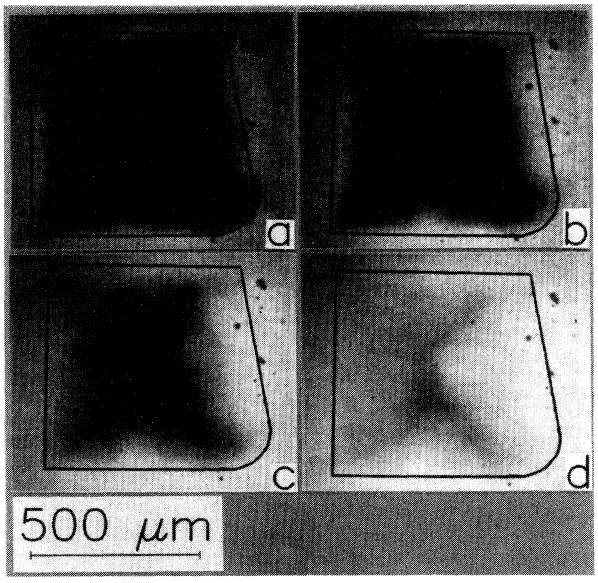

FIG. 5. Flux penetration into a cross-irradiated DBCO single crystal. The crystal was irradiated with 0.9-GeV Pb ions at $\varphi = \pm45°$, $\phi t = 1 \times 10^{10}$ ions/cm^2. The flux distributions were obtained using an iron-garnet indicator at $T = 60$ K and applied perpendicular fields of (a) $\mu_0 H_a = 43$ mT, (b) 85 mT, (c) 128 mT, and (d) 213 mT.

etrates deeper into the sample from the left and right than from the upper and lower edges; see Fig. 5(d). Thus the double-Y structure of the d lines is centered in the sample and oriented perpendicular to the longer crystal sides, whereas in the unirradiated sample the double-Y structure is aligned with them showing an isotropic current distribution. The anisotropy ratio after irradiation is determined as $j_{\parallel}/j_{\perp} = 1.55$.

In order to obtain information about the temperature dependence of the pinning behavior we investigate the full penetration field $H^* = j_c d$ of the DBCO crystals presented here. In this investigation our experimental setup imposes an upper limit to the field range of $\mu_0 H_a = 550$ mT due to the copper solenoid coil and a lower limit of 2 mT due to the sensitivity of the iron-garnet indicator.

The plot $H^*(T)$ is depicted in Fig. 6. For parallel angular irradiation H^* is much larger at low T's than for crossed LD's, but it drops faster with increasing T. Note that the fluence for parallel irradiation was more than 10 times higher than for crossed irradiation. For the fluences used we find an intersection of both curves at $T = 65$ K; if the same fluences were used for introduction of parallel and crossed LD's, the curve $H^*(T)$ obtained from cross-irradiated single crystals would always be located *above* the one obtained from the parallel-irradiated crystals, and an intersection does not occur. The $H^*(T)$ data for the unirradiated samples which drop to 0 already at $T \approx 50$ K are typical for all our DBCO single crystals.

The corresponding critical states for the cross-irradiated sample are shown in Fig. 7 for (a) $T = 30$ K and $\mu_0 H_a = 363$ mT, (b) 40 K and 288 mT, (c) 50 K and 235 mT, (d) 55 K and 213 mT, (e) 60 K and 181 mT, (f) 65 K and 160 mT, (g) 70 K and 128 mT, and (h) 75 K and 96 mT. Additionally to the above discussed T dependence of H^* we see a change in the d-line structure, i.e., in the anisotropy ratio $j_{\parallel}/j_{\perp}$. In the investigated field range we can safely neglect the B dependence of $j_{\parallel}/j_{\perp}$ because in increasing H_a over H^* at fixed T we do not observe a change of the d-line structure. Thus, the change of $j_{\parallel}/j_{\perp}$ is attributed to different T dependences of $j_{\parallel}$ and $j_{\perp}$. The curve $j_{\parallel}/j_{\perp}(T)$ is plotted in Fig. 8.

The above data are explained by Fig. 4. Figure 4(a) shows that sliding kinks are trapped by intersections of

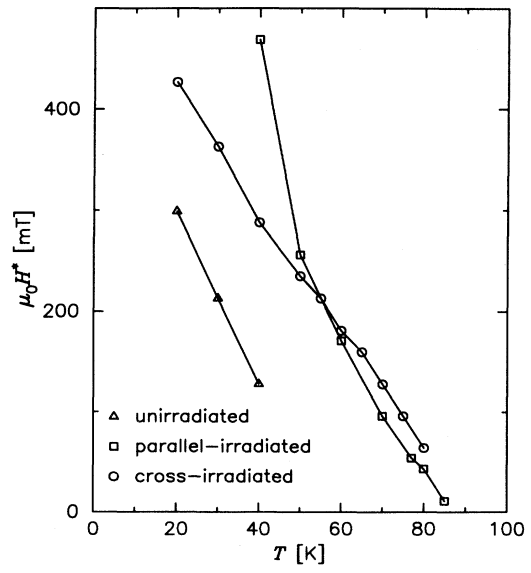

FIG. 6. Temperature dependence of the full penetration field H^* for an unirradiated (△), a parallel-irradiated ($\phi t = 1.29 \times 10^{11}$ ions/cm^2, □), and a cross-irradiated ($\phi t = 1.0 \times 10^{10}$ ions/cm^2, ○) DBCO single crystal.

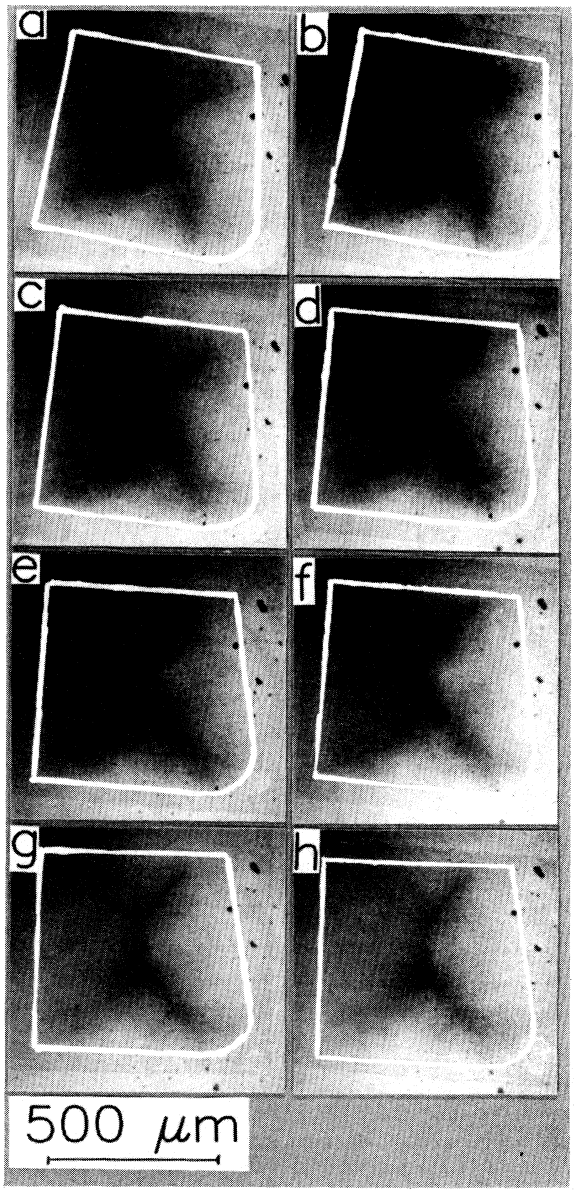

FIG. 7. Flux distributions in the critical states in the cross-irradiated DBCO single crystal at various temperatures. (a) $T = 30$ K, $\mu_0 H_a = 363$ mT, (b) 40 K, 288 mT, (c) 50 K, 235 mT, (d) 55 K, 213 mT, (e) 60 K, 181 mT, (f) 65 K, 160 mT, (g) 70 K, 128 mT, and (h) 75 K, 96 mT. From these flux distributions the T dependence of $j_{\parallel}/j_{\perp}$ was determined; see Fig. 8.

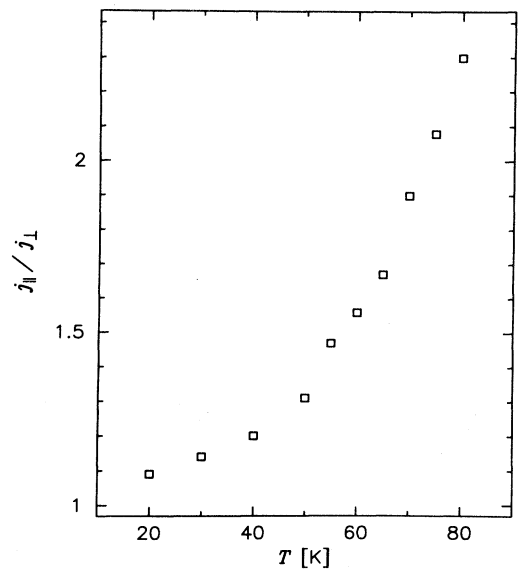

FIG. 8. Temperature dependence of the anisotropy ratio $j_\parallel/j_\perp$ of a cross-irradiated DBCO single crystal. The ratio $j_\parallel/j_\perp$ strongly increases with T showing the different T dependences of $j_\parallel$ and $j_\perp$.

LD's. These traps exclude the migration of surface kinks as a relevant depinning process; this can also be concluded from the observation that the anisotropy of $j_\perp$, which was attributed to surface effects, has disappeared; see Figs. 5(d) and 7. If kink sliding is stopped, the FL's are pinned in their full length by the LD's; see Fig. 4(b). Depinning now proceeds only by kink-pair formation, which results in a much higher activation barrier. Thus, the activation energy of FL's pinned by crossed LD's becomes similar to the considerations by Brandt[46] and in the Bose-glass model,[16,21] and the irradiation-enhanced critical currents are considerably larger than for parallel irradiation at the same fluence. In Fig. 4(b) we see that we have to distinguish two arrangements of FL's which are curved *against* (FL 1) and *with* (FL 2) the FL motion, respectively. During depinning at the intersection of the LD's, FL 1 is straightened (depinning mode A); this yields a lower activation energy than with the depinning mode C, where the FL 2 has to be considerably more curved and stretched; see the dashed lines. Depinning by kink-pair nucleation (mode B) is equivalent for all directions of vortex motion and requires an intermediate activation energy. Thus, FL 1 is depinned easily by mode A while FL 2 is not depinned by mode C since this requires the highest activation energy and is therefore not relevant for flux motion. Instead, FL 2 is depinned at another intersection of LD's where mode A can occur (the FL's form a zigzag line through the crossed LD's). For FL motion perpendicular to the inclination plane the FL's depin by mode B, which needs an intermediate activation energy. Therefore, the anisotropy of $j_\parallel/j_\perp$ in presence of crossed LD's is caused by the different activation energies for vortex motion perpendicular and parallel to the inclination direction of the LD's. This explains the observed increase of $j_\parallel/j_\perp$ with increasing T; see Fig. 8.

C. Parallel and crossed linear defects in Bi2212

In order to investigate FL depinning from LD's in a more anisotropic FL system we performed the same experiment as described in Secs. III A and III B on Bi2212 single crystals where the FL's decouple into pancake vortices.[13] For both parallel inclined and crossed irradiation we find an enhancement of j_c and a shift of the IL from about $T_{\rm irr} = 30$ K up to $T_{\rm irr} \approx 70$ K for ($\phi t = 1.29 \times 10^{11}$ ions/cm^2, $\varphi = 45°$; 500-MeV Xe) and $T_{\rm irr} \approx 80$ K for crossed irradiation ($\phi t = 1.0 \times 10^{10}$ ions/cm^2, $\varphi = \pm 45°$; 0.9-GeV Pb). Similarly to the experiments on DBCO the j_c enhancement due to crossed irradiation is much higher than for parallel inclined irradiation at the same fluence. However, in both cases we do not observe an anisotropy of the critical current flowing parallel or perpendicular to the inclination direction of the LD's. These results can be explained by the pancake structure of the FL's; see Fig. 9. The pancake vortices are more effectively pinned by the LD's than by the background pinning centers. The motion of pancake vortices is then initiated by one pancake which overcomes the pinning potential and jumps into the next LD. After this hopping process the neighboring pancakes can depin more easily and the motion of the imaginary line connecting the pancakes (dotted line) is similar to the kink motion along the LD's discussed in Sec. III A. However, now the potential barrier for initial hopping is the same for the two inclinations of the LD's with or against the direction of vortex motion [cf. the surface–kink-nucleation modes A, B, and C in Fig. 3(b)], because the imaginary vortex line runs always parallel to the crystal plane between two LD's. This behavior is also predicted by the scaling approach for anisotropic materials by Blatter *et al.*[51] If we scale the angle $\varphi = 45°$ with the anisotropy factor $\gamma \approx 60$ for Bi2212, we obtain an effective inclination angle $\tilde{\varphi}$ from $\tan\tilde{\varphi} = \gamma^{-1}\tan\varphi \approx 1°$; for DBCO with $\gamma \approx 6$ this scaling would give an effective inclination angle of about 10°. Therefore, in Bi2212 vortex motion

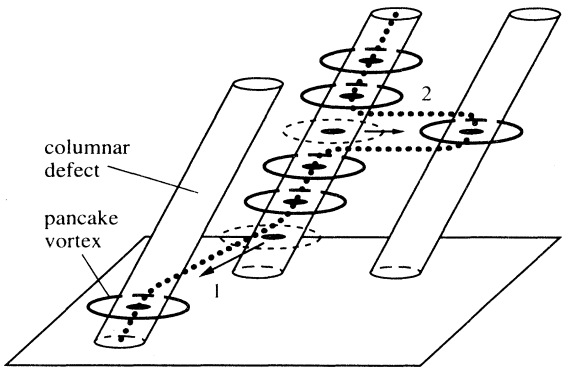

FIG. 9. Depinning of pancake vortices from inclined LD's. The vortex motion is initiated by a single pancake which jumps to the next LD. This hopping process is equivalent in all directions, especially for vortex motion perpendicular (1) and parallel (2) to the inclination direction.

in directions 1 and 2 is equivalent and an anisotropy of $j_{\parallel}/j_{\perp}$ cannot be observed. In the presence of parallel, inclined LD's the triggering hopping process occurs mainly at the sample surface, whereas for crossed LD's the vortex motion is initiated in the volume for the same reasons as given in Secs. III A and III B for kink motion in DBCO. As a consequence, the activation energy for vortex motion is higher in the presence of crossed LD's than it is for inclined parallel LD's.

D. Anisotropy ratio in DBCO during flux exit

A deviation from the anisotropic flux penetration discussed in Sec. III B occurs when the external field is decreased and the remanent state is reached. The flux distribution in the cross-irradiated DBCO single crystal presented in Fig. 5 during flux exit is shown in Fig. 10 for $T = 60$ K and external fields decreased from $\mu_0 H_a = 213$ mT [Fig. 5(d)] to (a) 149 mT, (b) 128 mT, (c) 85 mT, (d) 64 mT, (e) 43 mT, (f) 32 mT, (g) 21 mT, (h) 11 mT, and (i) the remanent state $H_a = 0$. The white frames indicate the sample edges and the sketches in the upper right corner of each picture are plotted to clarify the d-line structure. The double-Y structure is now imaged bright since in decreasing H_a the logarithmic infinities of the flux density, which occur at the sharp bends of the current flow (at the d lines), change their sign. At high fields [Figs. 10(a) and 10(d)] the observed anisotropy remains approximately the same as in increasing field [Figs. 5(d) and 10(e)]. More importantly, when H_a is further decreased the pattern of the d lines changes drastically: The central line of the double Y, which was oriented *parallel* to the shorter crystal sides, now shortens until the d lines running from the corners coincide with the diagonals of the sample; see Fig. 10(g). When the field is decreased further, the central d line grows again but now is oriented *perpendicular* to the shorter crystal sides. This means that the anisotropy ratio $j_{\parallel}/j_{\perp}$ decreases from 1.55 at $H_a = 213$ mT to 0.82 in the remanent state ($H_a = 0$) as can be seen in Fig. 11. The critical-current densities $j_{\parallel}$ and $j_{\perp}$ during field decrease are averaged over the critical-current distribution in each sector, which is not in general constant.

When the flux density has dropped to zero at the sample edges [Fig. 10(c)], a dark zone of zero-flux density spreads into the sample as H_a is further decreased. In the remanent state [Fig. 10(i)] the pinned FL's are visible only in the sample center whereas the dark zone of zero-flux density extends over the whole outer sample regions. However, the extended zone of zero-flux density in the outer sample regions does not necessarily imply that the magnetic moment should decrease with decreasing H_a. In the region of zero-flux density large currents even above the critical current[1] can flow. Due to the large distance from the sample center, these currents determine the magnetic moment. Furthermore, we observe that the d lines in the sample center become broader, but their intensities remain unchanged. This may mean an increase of the flux density there, which cannot be detected by a larger intensity because of the saturation of the video system (camera and image processor). The extended zone of low flux density during flux exit does not occur in unirradiated crystals. Here, reversed FL's penetrate the sample. The reversed FL's are separated from the pinned FL's in the sample center by a line at which the flux density is zero.[52] The different types of flux exit in irradiated and nonirradiated single crystals, which were observed also for parallel LD's perpendicular and inclined to the sample surface, are explained in Fig. 12.

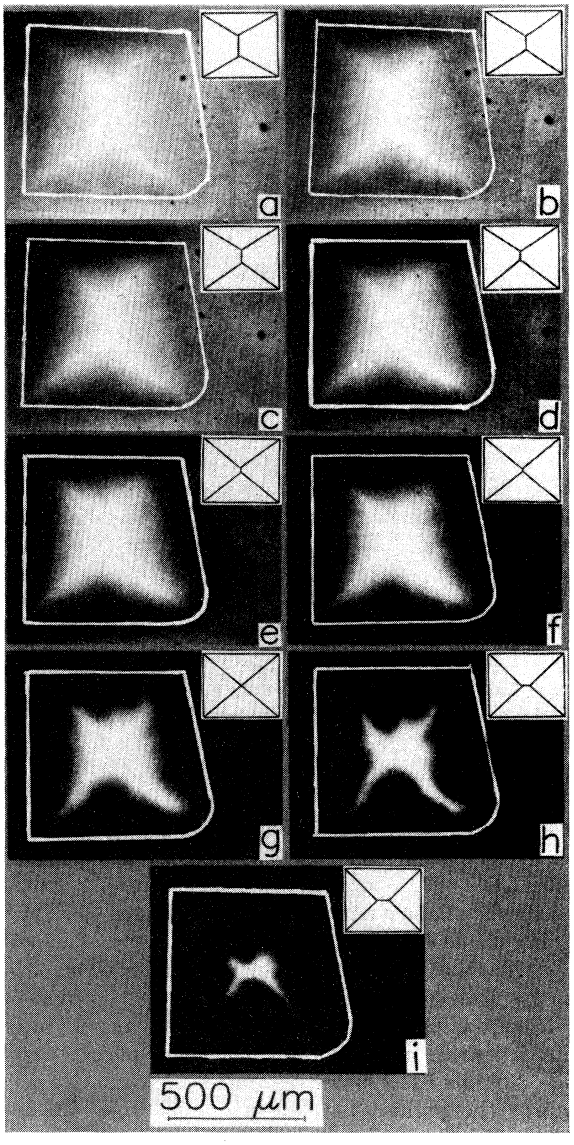

FIG. 10. Flux distributions obtained on the same cross-irradiated DBCO single crystal as shown in Fig. 5 during decrease of H_a from 213 mT at $T = 60$ K [see Fig. 5(d)]. The white frames indicate the sample edges and the small sketches in the upper right corners are the d-line structures for clarity. (a) 149 mT, (b) 128 mT, (c) 85 mT, (d) 64 mT, (e) 43 mT, (f) 32 mT, (g) 21 mT, (h) 11 mT, and (i) remanent state. Note that here the penetration of negative flux at low fields cannot be observed.

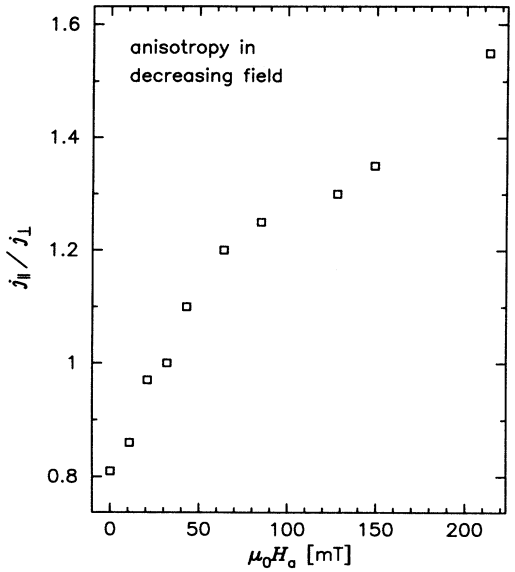

FIG. 11. Change of the anisotropy ratio $j_\parallel/j_\perp$ in decreasing H_a for the cross-irradiated sample shown in Fig. 5.

As depicted in Fig. 12(a) for parallel LD's oriented perpendicular to the sample surface the stray-field lines of the pinned FL's in the sample center form loops around the sample edges. The central line at which the stray field vanishes moves towards the sample center when H_a is decreased and FL's leave the sample. The FL's in the outer crystal regions are strongly inclined to the direction of the LD's by the stray field of the pinned FL's and even form closed loops in a region around the line $B = 0$. Kinks and antikinks move easily towards each other and annihilate as indicated by the arrows in Fig. 12(a); their motion is impeded only by the background pinning. Due to the strong curvature of the FL loops, intrinsic pinning of the kinks between two LD's at the Cu-O layers can safely be neglected. Thus, the FL loops collapse and a zone of zero-flux density remains, which extends from the sample edges to the pinned FL's in the center. In the outer region the critical-current density j_c is determined by the background pinning and it takes the value before irradiation. This consideration is valid for flux exit perpendicular to the LD's and for flux exit parallel to the inclination direction of parallel LD's as shown in Fig. 12(b). Thus, for inclined parallel LD's the anisotropy disappears in decreasing H_a and in the remanent state the distribution of the critical current is isotropic. The direct observation that during field decrease pinning by LD's becomes less effective and numerous LD's are no longer occupied by FL's (Ref. 53) supports our considerations.

The situation in cross-irradiated samples sketched in Fig. 12(c) is quite different. Whereas for flux exit perpendicular to the LD's we have the same behavior as described above, the FL loops parallel to the inclination direction are pinned by the "grid" of the LD's and the FL motion occurs as discussed in Sec. III B. Thus, the higher critical-current density $j_\parallel$ decreases in decreasing H_a to the value before irradiation, whereas $j_\perp$ remains almost unchanged because the collapse of FL loops is impeded by the intersections of the LD's. In this case the anisotropy ratio $j_\parallel/j_\perp$ reverses in the remanent state. However, due to the rescaled effective inclination angle $\tilde{\varphi} \approx 10°$, flux-line depinning parallel to the sample surface at the intersections of LD's is only slightly more difficult than depinning from parallel LD's, and thus the resulting reversed anisotropy ratio in the remanent state stays close to unity.

Figure 13 shows the penetration of reversed flux into the cross-irradiated DBCO single crystal starting from the remanent state depicted in Fig. 10(i) for (a) $\mu_0 H_a = -21$ mT, (b) $-$ 43 mT, (c) $-$ 64 mT, and (d) $-$ 85 mT. When the pinned FL's are annihilated by the entering reversed FL's the same flux-penetration behavior as described in Sec. III B for virgin magnetization is observed. This series shows that during field decrease and remagnetization two fronts penetrate the crystal: First,

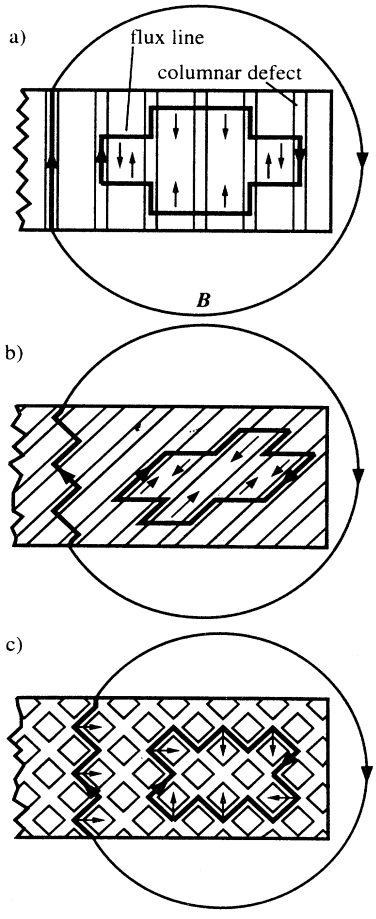

FIG. 12. (a) FL loops in parallel LD's which are oriented perpendicular to the sample surface. The kinks between pinned parts of a vortex loop can easily move through the crystal. Thus, kink and antikink move towards each other and annihilate and the vortex loop collapses. (b) FL loops in parallel, inclined LD's. (c) FL loops in crossed LD's. The flux lines are pinned by the LD's in the same way as described in Sec. III B and thus in low fields the anisotropy reverses.

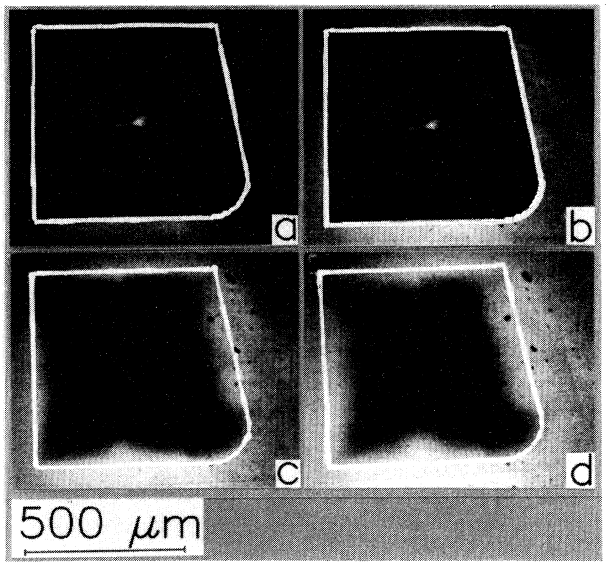

FIG. 13. Flux distributions in the cross-irradiated DBCO single crystal in reverse magnetic fields applied to the remanent state shown in Fig. 10(i). The observation temperature is 60 K. (a) $\mu_0 H_a = -21$ mT, (b) -43 mT, (c) -64 mT, and (d) -85 mT. After annihilation of the pinned FL's in the sample center the same flux-penetration behavior as for virgin magnetization is observed; see also Fig. 5.

in decreasing field the annihilation zone spreads from the sample edges towards the center and only during remagnetization does a front of reversed FL's penetrate the crystal. This behavior is in contrast to nonirradiated crystals where the reversed flux starts to penetrate when the flux density is zero at the sample edges, i.e., before the remanent state is reached.

IV. CONCLUSION

We investigated the B, T, and ϕt dependences of flux penetration and exit of DBCO and Bi2212 single crystals with parallel linear defects (LD's) which are inclined to the sample-surface normal, and with crossed LD's.

After introduction of parallel inclined LD's the DBCO single crystals show an anisotropic flux penetration from which we deduce the anisotropy ratio $j_\parallel/j_\perp \approx 2$ for the critical-current densities flowing parallel and perpendicular the the inclination plane of the LD's, respectively, at $T = 60$ K. This anisotropy ratio may be explained by different kink-nucleation modes of vortices at the sample surface, depending on the geometrical arrangement of the LD's and the surface and on the direction of FL motion. The observation that FL motion induced by $j_\perp$ differs for flux penetration from opposite sides supports this consideration. Additional experiments to demonstrate directly the influence of the sample surface on FL depinning are in progress.

For DBCO single crystals after introduction of crossed LD's we find an anisotropy $j_\parallel/j_\perp \approx 1.55$ at $T = 60$ K but a higher j_c enhancement than for parallel irradiation at the same fluence. This behavior is attributed to the effective pinning of sliding kinks at the intersections of the LD's. Therefore, FL's cannot depin by kink nucleation at the sample surface but only by kink-pair nucleation in the sample volume, which requires a higher energy. In this case the depinning energy is similar to that obtained by Brandt and in the Bose-glass model of Nelson and Vinokur. Again, the anisotropy $j_\parallel/j_\perp$ is due to the geometrical arrangements of the LD's, which form different angles in the different directions of FL motion. The higher pinning of cross-irradiated crystals compared with parallel-irradiated ones nicely confirms the results reported in Ref. 27.

During flux exit we find that the irradiation-induced anisotropy disappears in the case of parallel, inclined LD's and that it is even reversed in low fields for crossed LD's. This behavior is explained by the strongly curved FL's in decreasing field forced by the stray field of the pinned FL's in the sample center which causes FL's in the outer crystal regions to form loops. For parallel, inclined LD's the FL loops can easily collapse since kink motion is impeded only by the isotropic background pinning. In the case of crossed LD's the kink motion in the inclination plane is hindered by the "grid" of LD's where the FL loops are pinned, whereas for FL motion perpendicular to the inclination plane only the weaker background pinning determines $j_\parallel$ in decreasing field. This leads to the existence of an annihilation zone which extends from the sample edges to the pinned FL's in the center and the penetration of reversed FL's as observed in unirradiated HTSC's does not occur.

In Bi2212 single crystals we do not observe an anisotropic flux penetration either for parallel, inclined or for crossed LD's. This finding is explained in the framework of the pancake-vortex model where depinning of pancake vortices from LD's is equivalent in all directions. The crossed irradiation enhances the critical-current density more than parallel LD's produced by the same fluence.

The different behavior of DBCO and Bi2212 single crystals after introduction of parallel, inclined or crossed LD's is in good agreement with the scaling approach discussed by Blatter *at al.*[51] In this picture, when we scale the inclination angle φ with the anisotropy factor $\gamma \approx 60$ for Bi2212 we obtain an effective inclination angle of less than 1° and the j_c anisotropy disappears, whereas for DBCO ($\gamma \approx 6$) we have an effective inclination angle of about 10° which yields an observable j_c anisotropy.

ACKNOWLEDGMENTS

We wish to thank Professor H. Kronmüller and Professor G. Saemann-Ischenko for their constant interest in this work, E. H. Brandt for helpful discussions, and T. W. Li (Leiden University), A. A. Menovsky (University of Amsterdam), and the Dutch FOM (ALMOS) for the Bi2212 single crystals. Part of this work was financially supported by the Bundesministerium für Forschung und Technologie (Grant No. 13N6510) and the Bayerischer Forschungsverbund Hochtemperatur-Supraleitung FORSUPRA. This is gratefully acknowledged. One of us (M.I.) is grateful to Fond National Suisse de la Recherche Scientifique (FNPN30 Grant No. 4030-32794).

* Permanent address: Institute of Solid State Physics, Russian Academy of Sciences, Chernogolovka, 142432 Moscow, Russian Federation.

[1] Th. Schuster, M. V. Indenbom, H. Kuhn, E. H. Brandt, and M. Konczykowski, Phys. Rev. Lett. **73**, 1424 (1994); Th. Schuster, H. Kuhn, E. H. Brandt, M. V. Indenbom, M. R. Koblischka, and M. Konczykowski, Phys. Rev. B **50**, 16 684 (1994).

[2] E. H. Brandt, Phys. Rev. Lett. **77A**, 484 (1980).

[3] D. Bourgault, M. Hervieu, S. Bouffard, D. Groult, and B. Raveau, Nucl. Instrum. Methods B **42**, 61 (1989); B. Hensel, B. Roas, S. Henke, R. Hopfgärtner, M. Lippert, J. P. Ströbel, M. Vildic, and G. Saemann-Ischenko, Phys. Rev. B **42**, 4135 (1990); H. Watanabe, B. Kabius, K. Urban, B. Roas, S. Klaumünzer, and G. Saemann-Ischenko, Physica (Amsterdam) C **179**, 75 (1991); V. Hardy, D. Groult, M. Hervieu, J. Provost, B. Raveau, and S. Bouffard, Nucl. Instrum. Methods B **54**, 472 (1991); V. Hardy, J. Provost, D. Groult, M. Hervieu, B. Raveau, S. Durcok, E. Pollert, J. C. Frison, J. P. Chaminade, and M. Pouchard, Physica (Amsterdam) C **191**, 85 (1992); B. Chenevier, S. Ikeda, H. Kumakura, K. Togano, S. Okayasu, and Y. Kazumata, Jpn. J. Appl. Phys. **31**, L777 (1992).

[4] B. Roas, B. Hensel, S. Henke, S. Klaumünzer, and B. Kabius, Europhys. Lett. **11**, 669 (1990).

[5] L. Civale, A. D. Marwick, T. K. Worthington, M. A. Kirk, J. A. Thompson, L. Krusin-Elbaum, Y. Sun, J. R. Clem, and F. Holtzberg, Phys. Rev. Lett. **67**, 648 (1991).

[6] M. Konczykowski, F. Rullier-Albenque, E. R. Yacoby, A. Shaulov, Y. Yeshurun, and P. Lejai, Phys. Rev. B **44**, 7167 (1991).

[7] V. Hardy, D. Groult, J. Provost, and B. Raveau, Physica (Amsterdam) C **178**, 255 (1991).

[8] W. Gerhäuser, G. Ries, H.-W. Neumüller, W. Schmitt, O. Eibl, G. Saemann-Ischenko, and S. Klaumünzer, Phys. Rev. Lett. **68**, 879 (1992).

[9] M. Leghissa, Th. Schuster, W. Gerhäuser, S. Klaumünzer, M. R. Koblischka, H. Kronmüller, H. Kuhn, H.-W. Neumüller, and G. Saemann-Ischenko, Europhys. Lett. **11**, 323 (1992); Th. Schuster, M. R. Koblischka, H. Kuhn, H. Kronmüller, M. Leghissa, W. Gerhäuser, G. Saemann-Ischenko, H.-W. Neumüller, and S. Klaumünzer, Phys. Rev. B **46**, 8496 (1992).

[10] Th. Schuster, M. Leghissa, M. R. Koblischka, H. Kuhn, H. Kronmüller, and G. Saemann-Ischenko, Physica (Amsterdam) C **203**, 203 (1992).

[11] R. C. Budhani, Y. Zhu, and M. Suenaga, Appl. Phys. Lett. **61**, 985 (1992); V. Hardy, D. Groult, J. Provost, and B. Raveau, Physica (Amsterdam) C **190**, 289 (1992); Th. Schuster, H. Kuhn, M. R. Koblischka, H. Theuss, H. Kronmüller, M. Leghissa, M. Kraus, and G. Saemann-Ischenko, Phys. Rev. B **47**, 373 (1993); M. Leghissa, A. Königer, M. Lippert, W. Dorsch, M. Kraus, and G. Saemann-Ischenko, Z. Phys. B **92**, 163 (1993); L. Civale, A. D. Marvick, R. Wheeler IV, M. A. Kirk, W. L. Carter, G. N. Riley, and A. P. Malozemoff, Physica (Amsterdam) C **208**, 137 (1993).

[12] P. Kummeth, C. Struller, H.-W. Neumüller, G. Ries, M. Kraus, M. Leghissa, G. Wirth, J. Wiesner, and G. Saemann-Ischenko, J. Supercond. **7**, 783 (1994).

[13] J. R. Clem, Phys. Rev. B **43**, 7837 (1991); L. N. Bulaevskii, Sov. Phys. JETP **37**, 1133 (1973).

[14] M. Konczykowski, V. M. Vinokur, F. Rullier-Albanque, Y. Yeshurun, and F. Holtzberg, Phys. Rev. B **47**, 5531 (1993).

[15] L. Klein, E. R. Yacoby, Y. Wolfus, J. Yeshurun, L. Burlachkov, and B. Ya. Shapiro, Phys. Rev. B **47**, 12 349 (1993).

[16] D. R. Nelson and V. M. Vinokur, Phys. Rev. Lett. **68**, 2398 (1992).

[17] U. Essmann and H. Träuble, Phys. Lett. A **24**, 526 (1967); Sci. Am. **224** (3), 74 (1971).

[18] M. Leghissa, L. A. Gurevich, M. Kraus, G. Saemann-Ischenko, and L. A. Vinnikov, Phys. Rev. B **48**, 1341 (1993).

[19] H. Dai, S. Yoon, J. Liu, R. C. Budhani, and C. M. Lieber, Science **265**, 1552 (1994).

[20] I. F. Lyuksyutov, Europhys. Lett. **20**, 273 (1992).

[21] D. R. Nelson and V. M. Vinokur, Phys. Rev. B **48**, 13 060 (1993).

[22] T. Hwa, P. Le Doussal, D. R. Nelson, and V. M. Vinokur, Phys. Rev. Lett. **71**, 3545 (1993).

[23] W. Jiang, N.-C. Yeh, D. S. Reed, U. Kriplani, D. A. Beam, M. Konczykowski, T. A. Tombrello, and F. Holtzberg, Phys. Rev. Lett. **72**, 550 (1994); R. C. Budhani, W. L. Holstein, and M. Suenaga, *ibid.* **72**, 566 (1994); V. V. Moshchalkov, V. V. Metlushko, G. Güntherodt, I. N. Goncharov, A. Yu. Didyk, and Y. Bruynseraede, Phys. Rev. B **50**, 639 (1994).

[24] M. Kraus, G. Kreiselmeyer, J. Daniel, M. Leghissa, G. Saemann-Ischenko, B. Holzapfel, P. Kummeth, R. Scholz, and L. Ya. Vinnikov, Nucl. Instrum. Methods B **89**, 307 (1994).

[25] J. R. Thompson, Y. R. Sun, H. R. Kerchner, D. K. Christen, B. C. Sales, B. C. Chakoumakos, A. D. Marwick, L. Civale, and J. O. Thomson, Appl. Phys. Lett. **60**, 2306 (1992).

[26] L. Klein, E. R. Yacoby, Y. Yeshurun, M. Konczykowski, and K. Kishio, Phys. Rev. B **48**, 3523 (1993).

[27] L. Civale, L. Krusin-Elbaum, J. R. Thompson, R. Wheeler, A. D. Marvick, M. A. Kirk, Y. R. Sun, F. Holtzberg, and C. Feild, Phys. Rev. B **50**, 4102 (1994); L. Krusin-Elbaum, J. R. Thompson, R. Wheeler, A. D. Marwick, C. Li, S. Patel, D. T. Shaw, P. Lisowski, and J. Ullmann, Appl. Phys. Lett. **64**, 3331 (1994).

[28] R. Prozorov, A. Tsameret, Y. Yeshurun, G. Koren, M. Konczykowski, and S. Bouffard, Physica (Amsterdam) C **234**, 311 (1994).

[29] B. Holzapfel, G. Kreiselmeyer, M. Kraus, G. Saemann-Ischenko, S. Bouffard, S. Klaumünzer, and L. Schultz, Phys. Rev. B **48**, 600 (1993).

[30] T. Hwa, D. R. Nelson, and V. M. Vinokur, Phys. Rev. B **48**, 1167 (1993).

[31] Th. Schuster, M. V. Indenbom, H. Kuhn, H. Kronmüller, M. Leghissa, and G. Kreiselmeyer, Phys. Rev. B **50**, 9499 (1994).

[32] Th. Schuster, M. R. Koblischka, N. Moser, B. Ludescher, and H. Kronmüller, Cryogenics **31**, 811 (1991).

[33] R. P. Huebener, *Magnetic Flux Structures in Superconductors* (Springer, New York, 1979).

[34] M. V. Indenbom, Th. Schuster, M. R. Koblischka, A. Forkl, H. Kronmüller, L. A. Dorosinskii, V. K. Vlasko-Vlasov, A. A. Polyanskii, R. L. Prozorov, and V. I. Nikitenko, Physica (Amsterdam) C **209**, 259 (1993).

[35] L. A. Dorosinskii, M. V. Indenbom, V. I. Nikitenko, Yu. A. Ossip'yan, A. A. Polyanskii, and V. K. Vlasko-Vlasov, Physica (Amsterdam) C **203**, 149 (1992).

[36] K.-H. Greubel, E. Gmelin, N. Moser, Ch. Mensing, and L. Walz, Cryogenics Suppl. **30**, 457 (1990).

[37] M. R. Koblischka, N. Moser, B. Gegenheimer, and H. Kronmüller, Physica (Amsterdam) C **166**, 36 (1990).
[38] T. W. Li, P. H. Kes, N. T. Hien, J. J. M. Franse, and A. A. Menovsky, J. Cryst. Growth **135**, 481 (1994).
[39] C. Thomsen, M. Cardona, B. Gegenheimer, R. Liu, and R. Simon, Phys. Rev. B **37**, 9860 (1988).
[40] L. Dorosinskii, B. Farber, M. Indenbom, V. Nikitenko, A. Polyanskii, and V. Vlasko-Vlasov, Ferroelectrics **111**, 321 (1990).
[41] V. A. Rowe, R. P. Huebener, and T. Kampwirth, Phys. Status Solidi A **4**, 513 (1971); P. Brüll, D. Kirchgässner, and P. Leiderer, Physica (Amsterdam) C **182**, 339 (1991); V. K. Vlasko-Vlasov, M. V. Indenbom, R. L. Prozorov, I. V. Grekhov, L. A. Delimova, I. A. Liniichuk, A. V. Antonov, and M. Yu. Gusev, Superconductivity **5**, 1584 (1992); E. H. Brandt (unpublished).
[42] H. A. M. van den Berg, J. Appl. Phys. **60**, 1104 (1986).
[43] A. M. Campbell and J. E. Evetts, *Critical Currents in Superconductors* (Taylor & Francis, London, 1972), p. 71; in *Concise Encyclopedia of Magnetic and Superconducting Materials*, edited by J. Evetts (Pergamon, Oxford, 1992).
[44] Th. Schuster, M. V. Indenbom, M. R. Koblischka, H. Kuhn, and H. Kronmüller, Phys. Rev. B **49**, 3443 (1994).
[45] E. M. Gyorgy, R. B. van Dover, K. A. Jackson, L. F. Schneemeyer, and J. V. Waszack, Appl. Phys. Lett. **55**, 283 (1989); F. M. Sauerzopf, A. P. Wiesinger, and H. W. Weber, Cryogenics **30**, 650 (1990).
[46] E. H. Brandt, Europhys. Lett. **18**, 635 (1992); Phys. Rev. Lett. **69**, 1105 (1992).
[47] J. R. Clem, J. Low Temp. Phys. **38**, 353 (1980); Physica B **107**, 453 (1980).
[48] E. H. Brandt, J. Low Temp. Phys. **39**, 41 (1980); A. Sudbø and E. H. Brandt, Phys. Rev. Lett. **66**, 1781 (1991).
[49] M. V. Indenbom, A. Forkl, B. Ludescher, H. Kronmüller, H.-U. Habermeier, B. Leibold, G. D'Anna, T. W. Li, P. H. Kes, and A. A. Menovsky, Physica (Amsterdam) C **226**, 325 (1994).
[50] Th. Schuster, M. R. Koblischka, B. Ludescher, and H. Kronmüller, J. Appl. Phys. **72**, 1478 (1992); A. I. Belyaeva, S. V. Voitsenya, V. P. Yur'ev, M. A. Obolenskii, and A. V. Bondarenko, Superconductivity **5**, 1406 (1992); C. A. Duran, P. L. Gammel, R. Wolf, V. J. Fratello, D. J. Bishop, J. P. Rice, and D. M. Ginsberg, Nature **357**, 474 (1992); V. K. Vlasko-Vlasov, M. V. Indenbom, and A. A. Polyanskii, in *The Real Structure of High-T_c Superconductors*, edited by V. Sh. Shekhtman, Springer Series in Materials Science Vol. 23 (Springer, Berlin, 1993), pp. 111–144; A. I. Belyaeva, S. V. Voitsenya, V. P. Yuriyev, M. A. Obolenskii, and A. V. Bondarenko, Solid State Commun. **55**, 427 (1993); M. Turchinskaya, D. L. Kaiser, F. M. Gayle, A. J. Shapiro, A. Roytburd, V. Vlasko-Vlasov, A. Polyanskii, and V. Nikitenko, Physica (Amsterdam) C **216**, 205 (1993).
[51] G. Blatter, V. B. Geshkenbein, and A. I. Larkin, Phys. Rev. Lett. **68**, 875 (1992).
[52] R. Szymczak, K. Piotrowski, H. Szymczak, and A. M. Balbashov, J. Magn. Magn. Mater. **92**, L19 (1990); Th. Schuster, M. R. Koblischka, N. Moser, and H. Kronmüller, Physica (Amsterdam) C **179**, 269 (1991); A. Forkl, H.-U. Habermeier, B. Leibold, T. Dragon, and H. Kronmüller, *ibid.* **180**, 155 (1991); Th. Schuster, M. R. Koblischka, H. Kuhn, B. Ludescher, M. Leghissa, M. Lippert, and H. Kronmüller, *ibid.* **196**, 373 (1992).
[53] S. Behler, S. H. Pan, P. Jess, A. Baratoff, H. J. Güntherodt, F. Lévy, G. Wirth, and J. Wiesner, Phys. Rev. Lett. **72**, 1750 (1994).

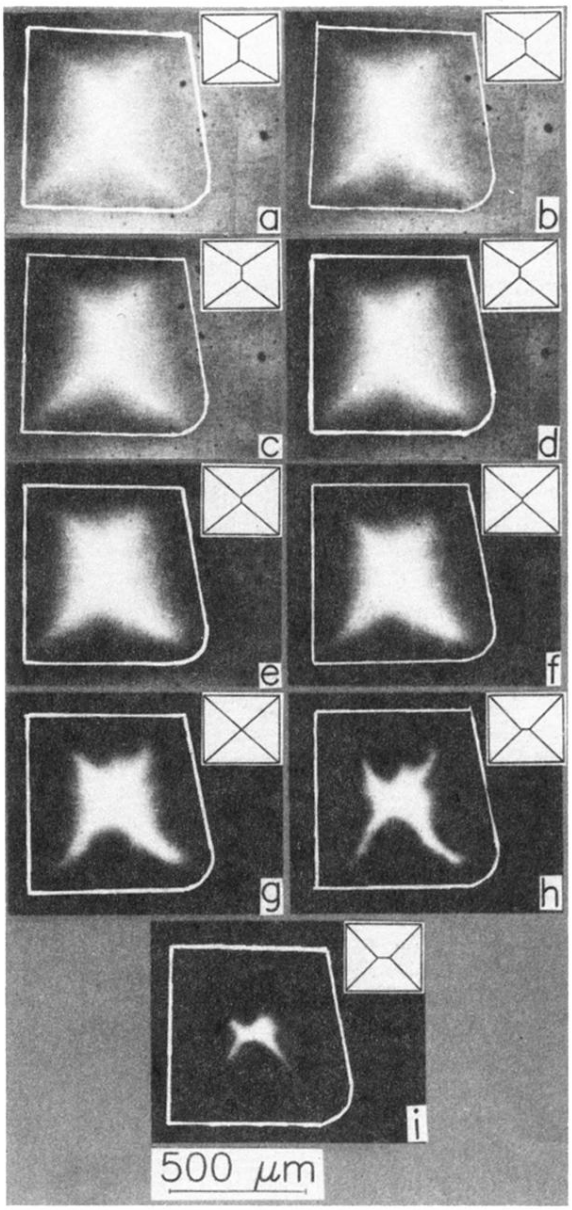

FIG. 10. Flux distributions obtained on the same cross-irradiated DBCO single crystal as shown in Fig. 5 during decrease of H_a from 213 mT at $T = 60$ K [see Fig. 5(d)]. The white frames indicate the sample edges and the small sketches in the upper right corners are the d-line structures for clarity. (a) 149 mT, (b) 128 mT, (c) 85 mT, (d) 64 mT, (e) 43 mT, (f) 32 mT, (g) 21 mT, (h) 11 mT, and (i) remanent state. Note that here the penetration of negative flux at low fields cannot be observed.

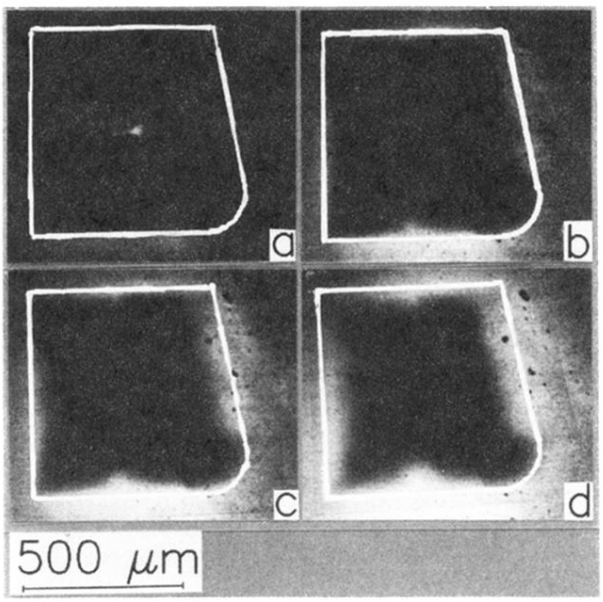

FIG. 13. Flux distributions in the cross-irradiated DBCO single crystal in reverse magnetic fields applied to the remanent state shown in Fig. 10(i). The observation temperature is 60 K. (a) $\mu_0 H_a = -21$ mT, (b) -43 mT, (c) -64 mT, and (d) -85 mT. After annihilation of the pinned FL's in the sample center the same flux-penetration behavior as for virgin magnetization is observed; see also Fig. 5.

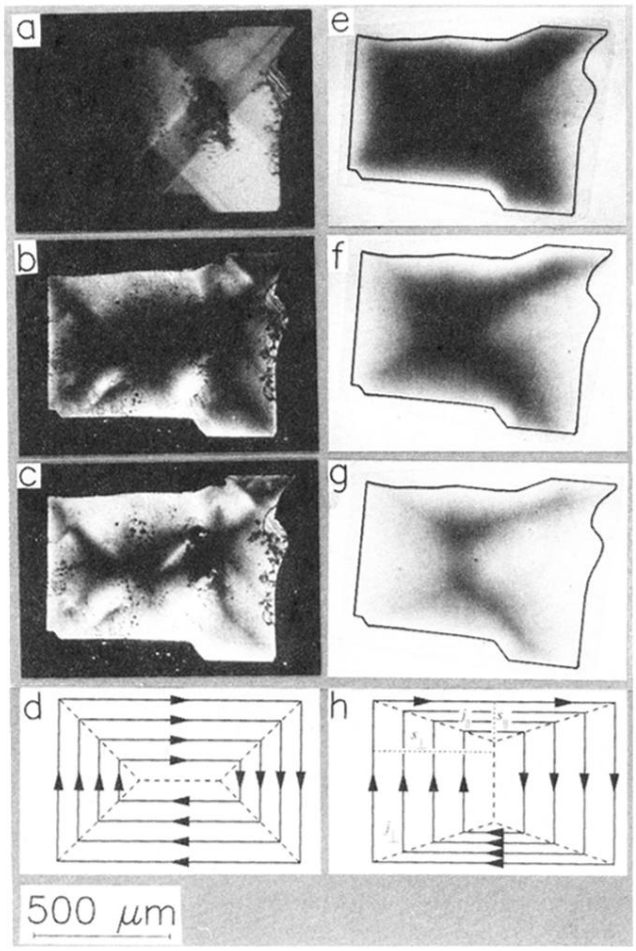

FIG. 2. Flux distributions in a DBCO single crystal before and after irradiation with 500-MeV Xe ions at $\varphi = 45°$ and $\phi t = 1.29 \times 10^{11}$ ions/cm^2. The observation temperature is $T = 30$ K before (b), (c) and $T = 60$ K after irradiation (e)–(g). (a) Polarization micrograph of the crystal surface before coating with the Al and EuSe layers. The twin structure is visible as straight lines running at 45° to the sample edges. (b) $\mu_0 H_a = 171$ mT, (c) 256 mT. The flux distributions before irradiation were visualized using a EuSe thin film. (d) Isotropic current distribution in a rectangular sample in the critical state. (e) $\mu_0 H_a = 85$ mT. The flux distributions after irradiation were revealed using a ferrimagnetic iron-garnet indicator. (f) 171 mT, (g) 256 mT, (h) anisotropic current distribution in a rectangular sample. The ratio $j_\parallel / j_\perp$ of the critical currents flowing parallel or perpendicular to the LD's can be determined by measuring the distances $s_\parallel$ and $s_\perp$.

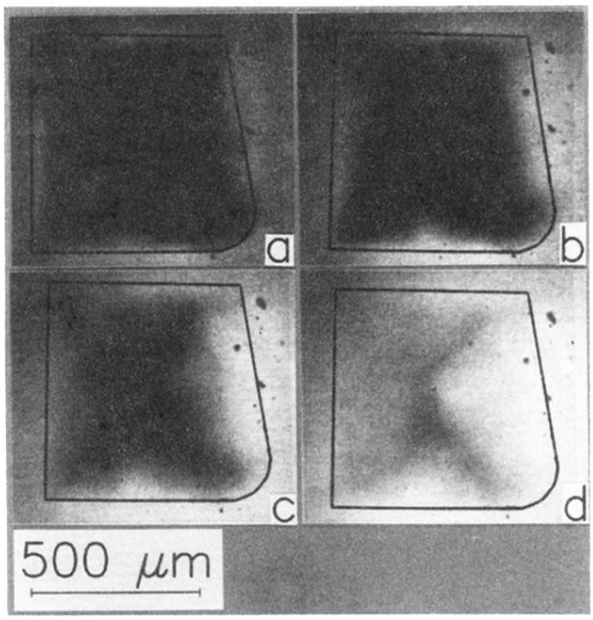

FIG. 5. Flux penetration into a cross-irradiated DBCO single crystal. The crystal was irradiated with 0.9-GeV Pb ions at $\varphi = \pm 45°$, $\phi t = 1 \times 10^{10}$ ions/cm^2. The flux distributions were obtained using an iron-garnet indicator at $T = 60$ K and applied perpendicular fields of (a) $\mu_0 H_a = 43$ mT, (b) 85 mT, (c) 128 mT, and (d) 213 mT.

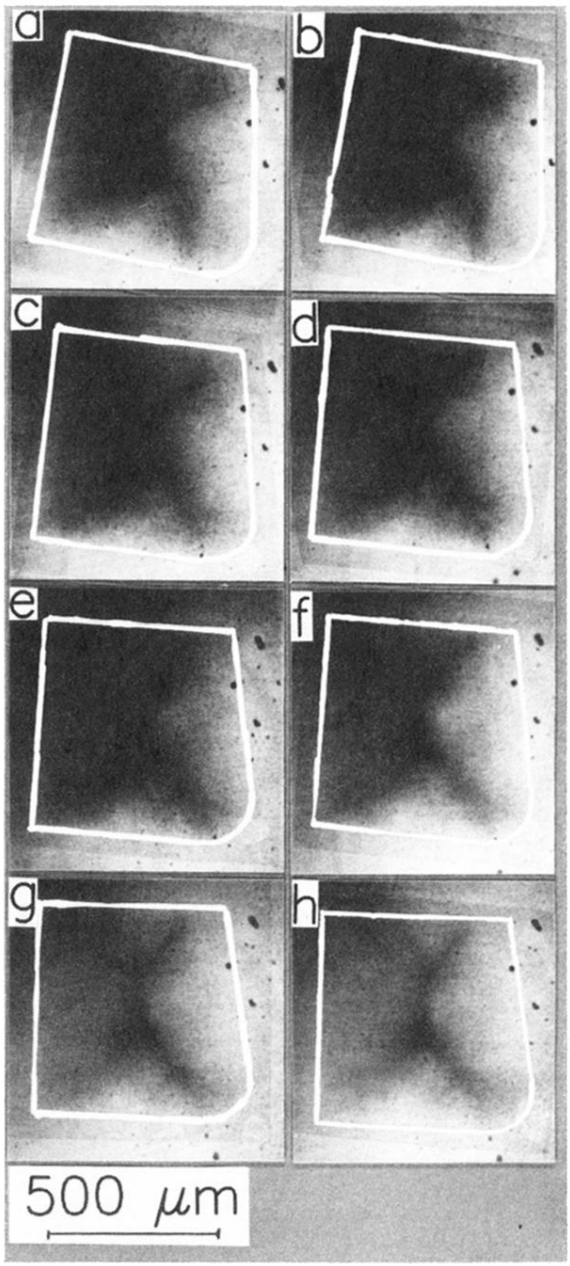

FIG. 7. Flux distributions in the critical states in the cross-irradiated DBCO single crystal at various temperatures. (a) $T = 30$ K, $\mu_0 H_a = 363$ mT, (b) 40 K, 288 mT, (c) 50 K, 235 mT, (d) 55 K, 213 mT, (e) 60 K, 181 mT, (f) 65 K, 160 mT, (g) 70 K, 128 mT, and (h) 75 K, 96 mT. From these flux distributions the T dependence of $j_\parallel/j_\perp$ was determined; see Fig. 8.